ELSEVIER

Chemical Physics 273 (2001) 235–248

Chemical Physics

www.elsevier.com/locate/chemphys

Picosecond absorption anisotropy of polymethine and squarylium dyes in liquid and polymeric media

Olga V. Przhonska [a,b], David J. Hagan [a,*], Evgueni Novikov [a], Richard Lepkowicz [a], Eric W. Van Stryland [a], Mikhail V. Bondar [b], Yuriy L. Slominsky [c], Alexei D. Kachkovski [c]

[a] *School of Optics/CREOL (Center for Research and Education in Optics and Lasers), University of Central Florida, Orlando, FL 32816-2700, USA*

[b] *Institute of Physics, National Academy of Sciences of Ukraine, Prospect Nauki 46, Kiev-28 03028, Ukraine*

[c] *Institute of Organic Chemistry, National Academy of Sciences of Ukraine, Murmanskaya str. 5, Kiev-94 02094, Ukraine*

Received 9 July 2001

Abstract

Time-resolved excitation-probe polarization measurements are performed for polymethine and squarylium dyes in ethanol and an elastopolymer of polyurethane acrylate (PUA). These molecules exhibit strong excited-state absorption in the visible, which results in reverse saturable absorption (RSA). In pump–probe experiments, we observe a strong angular dependence of the RSA decay kinetics upon variation of the angle between pump and probe polarizations. The difference in absorption anisotropy kinetics in ethanol and PUA is detected and analyzed. Anisotropy decay curves in ethanol follow a single exponential decay leading to complete depolarization of the excited state. We also observe complete depolarization in PUA, in which case the anisotropy decay follows a double exponential behavior. Possible rotations in the PUA polymeric matrix are connected with the existence of local microcavities of free volume. We believe that the fast decay component is connected with the rotation of molecular fragments and the slower decay component is connected with the rotation of entire molecules in local microcavities, which is possible because of the elasticity of the polymeric material. © 2001 Published by Elsevier Science B.V.

1. Introduction

Over the past several years our efforts have been directed toward a systematic investigation of nonlinear properties of a new series of polymethine dyes (PDs) and squarylium dyes (SDs) in liquid solutions and polymeric media [1,2]. We were able to systematically modify the photophysical properties of the dyes through changes in their molecular structure. These studies led to the development of several new dyes showing strong excited-state absorption (ESA) in the visible spectral region with the ratios of excited- to ground-state absorption cross-sections up to 200 at 532 nm. One of the important applications of ESA is for optical limiting devices that protect human eyes and sensitive optical components from laser-induced damage [3,4].

Further development and optimization of organic molecules with large ESA requires a detailed

* Corresponding author. Fax: +1-407-823-6880.
E-mail address: hagan@creol.ucf.edu (D.J. Hagan).

0301-0104/01/$ - see front matter © 2001 Published by Elsevier Science B.V.
PII: S0301-0104(01)00481-5

investigation of excited-state dynamics and molecular motions in different micromolecular environments. Picosecond pump–probe methods have been extensively used to measure ground or excited-state decay kinetics for solutions of many organic molecules since 1970–1980s. In the series of articles by Lessing and Von Jena [5–7] it was shown both theoretically and experimentally that transient absorption measurements reflect electronic level decay kinetics and rotational relaxations. A rotation-independent measurement is realized if the angle between the polarizations of the pump and probe beam reaches 54.7° (the "magic angle").

The goal of this work is to understand the nature of rotational motions of excited molecules of PDs and SDs in liquid (ethanol) solutions and polymeric media and their effect on ESA. For this purpose we performed picosecond pump–probe polarization measurements and analyzed the anisotropy of the nonlinear response.

Fluorescence anisotropy methods, both steady state and time resolved, are now extensively used for studying the dynamics and mechanisms of molecular motions in solutions in different areas of physics, chemistry, and molecular biology [8]. There are only a limited number of studies on anisotropy in dye-doped synthetic polymers [9–11]. The main results support the assumption that in polymers the rotational motions are not restricted by the viscosity of the micromolecular environment as in frozen solutions but strongly depend on the local free volume of the polymer network, size of the molecular probes and specific interaction effects.

It has been shown that anisotropy methods may also be applied to transient pump–probe spectroscopy [12–14]. These methods are not only complementary to fluorescence anisotropy measurements but frequently provide more direct information about the dynamics of the induced anisotropy, which depends upon the rotational and conformation kinetics.

From the experiments reported here we observe that the anisotropy decays completely for all dyes measured, both in ethanol solution and in the polymeric host matrix, polyurethane acrylate (PUA). The anisotropy for the dyes in ethanol follows a single exponential decay, while in PUA it follows a double exponential behavior. We discuss the most likely reorientation mechanisms in ethanol and the polymeric matrix.

2. Experimental section

2.1. Materials

The molecular structures of the dyes studied in this article are shown in Fig. 1. Polymethine dye 2-[2-[3-[(1,3-dihydro-3,3-dimethyl-1-phenyl-2H-indol-2-ylidene)ethylidene]-2-phenyl-1-cyclohexen-1-yl]ethenyl]-3,3-dimethyl-1-phenylindolium perchlorate (labeled as PD #2093) and squarylium dye 1,3-bis-[(1,3-dihydro-1-butyl-3,3-dimethyl-2H-benzo[e]indol-2-ylidene)methyl]squaraine (labeled as SD #2243) were synthesized at the Institute of Organic Chemistry, Kiev, Ukraine. All experiments were performed in two host media: absolute ethanol and an elastopolymer PUA. The polymeric samples were prepared by a previously reported radical photopolymerization procedure [2,15]. The room temperature linear absorption

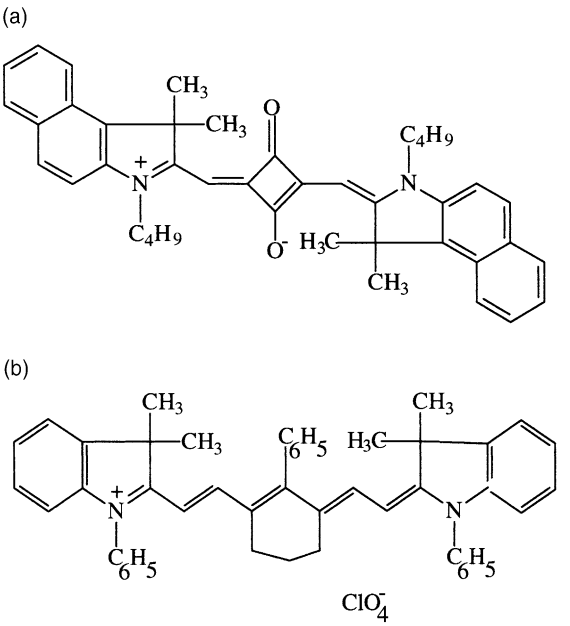

Fig. 1. Molecular structure of (a) SD #2243 and (b) PD #2093.

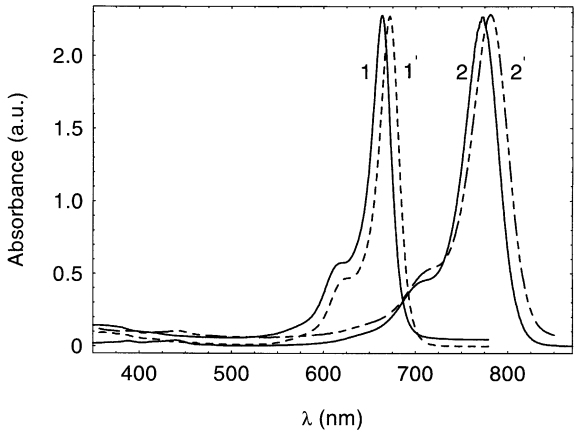

Fig. 2. Linear absorption spectra of SD #2243 (1, 1′) and PD #2093 (2, 2′) in ethanol (solid lines 1 and 2) and PUA (dashed lines 1′ and 2′).

spectra presented in Fig. 2 were recorded with a Varian Cary 500 spectrophotometer.

The spectroscopic and nonlinear optical properties of PD #2093 are determined by the existence of the delocalized π-electron systems in the polymethine chromophore and symmetric terminal groups. Inclusion of a 6-link cycle with phenyl substitute in the polymethine chromophore shifts the absorption maximum by 15 nm to the red region with respect to its unsubstituted analogue. The linear absorption maximum occurs at 770 nm in ethanol and at 781 nm in PUA. As was shown in our previous article [2], PD #2093 is one of the best reverse saturable absorption (RSA) dyes for optical limiting, both in ethanol and PUA. The ESA cross-section in ethanol at 532 nm, $\sigma_{ex} = 3 \times 10^{-16}$ cm^2 while keeping a large enough ground-state absorption, $\sigma_{01} = 1.5 \times 10^{-18}$ cm^2.

The main distinguishing features of SD #2243 are the existence of the central "square" group C_4O_2 and the long tails C_4H_9 connected to nitrogen atoms at the end of the chromophore. In comparison with PDs, SDs are neutral with a localization of positive charge occurring on the nitrogen atom and of negative charge on the oxygen atom of the central group. Most SDs are characterized by large extinction coefficients and narrow absorption bands of the $S_0 \rightarrow S_1$ transitions. The long C_4H_9 butyl tails improve the solubility of the dye both in ethanol and in the PUA matrix and prevent formation of aggregates even at large concentrations, up to (1.5–2) $\times 10^{-3}$ M/l. The linear absorption maximum for SD #2243 is placed at 663 nm in ethanol and at 672 nm in PUA. The nonlinear optical properties of this dye are described below in Section 3.1. The intense and broadband ESA for this dye in the visible spectral range was reported by us recently [16]. PD #2093 and SD #2243 are relatively photochemically stable for optical limiting applications both in ethanol and PUA [2]. Quantum-chemical geometry optimization of PD #2093 and SD #2243 was performed with the AM1 semiempirical method using the HyperChem software package. Transition energies and dipole moments as well as atomic charges in the ground and excited states were calculated with ZINDO/S approximation.

2.2. Experimental methods

Picosecond pump–probe measurements and *Z*-scan nonlinear characterization of the liquid and polymeric samples were performed using a frequency doubled, active/passive modelocked, 10 Hz repetition rate, Nd:YAG laser (1064 nm). This produces a 40 ns train of pulses each separated by 7 ns, from which a single pulse is switched out. After frequency doubling to 532 nm, the pulsewidth is measured to be 30 ps (FWHM). In the pump–probe measurements a strong, linearly polarized pump pulse is incident on the sample. Those molecules with transition dipole moment aligned parallel to the pump polarization will be more likely to be excited. Therefore the excited-state population, and hence the ESA, is anisotropic. By varying the polarization of the probe beam, we can sense the anisotropy of the ESA. In our experiments, both pump and probe were at a wavelength of 532 nm. The pump and probe beams were focused to waists of radius 230 and 35 μm ($HW1/e^2M$), respectively. The range of pumping energies was 0.7–2 μJ. The probe beam was delayed up to 15 ns and its irradiance was kept much smaller that that of the pump, so as not to induce any significant nonlinearity. Pump and probe beams were overlapped at a small angle (<5°) within the sample. The measurements were performed for probe pulses polarized along several

angles ranging from parallel to perpendicular to the pump beam (0°, 18°, 36°, "magic angle" 54.7°, 72° and 90°).

In open aperture *Z*-scans the total energy transmitted by the sample was measured as it is axially scanned through a focal plane, while holding the energy constant [4]. In our experiments, the 532 nm beam was focused to a measured waist of radius 20 μm ($HW1/e^2M$).

3. Results

3.1. Nonlinear characterization of SD #2243

We studied the nonlinear transmittance at 532 nm of SD #2243 in "open aperture" *Z*-scans over a range of input energies from 0.01 μJ (where the nonlinear response is weak) to 0.065 μJ (much less than the level of photodegradation of the dye under repeated irradiation). These data are shown in Fig. 3. Irradiation at 532 nm produces an excitation into the short wavelength tail of the linear absorption band. Here the ground-state absorption cross-section in ethanol, σ_{01} (532 nm) = 1.7×10^{-18} cm^2. This dye shows RSA which indicates that σ_{01} (532 nm) < σ_{ex} (532 nm). Fitting of *Z*-scan data shown in Fig. 3 has been performed using a 3-level model $S_0 \rightarrow S_1 \rightarrow S_{ex}$ (all singlet states), which adequately explains our picosecond results. Numerical fits make it possible to determine σ_{ex} (532 nm) as well as estimate the value of the lifetime τ_2 for the second excited state S_2. They are: σ_{ex} (532 nm) = 2.5×10^{-16} cm^2 and $\tau_2 = 2$ ps. This short but finite lifetime of the S_2 level limits the nonlinear response of the dye due to saturation of absorption from the first excited state. For ethanol solution the ratio of $\sigma_{ex}/\sigma_{01} \approx 150$ at 532 nm, which is much larger than for SDs reported earlier [2].

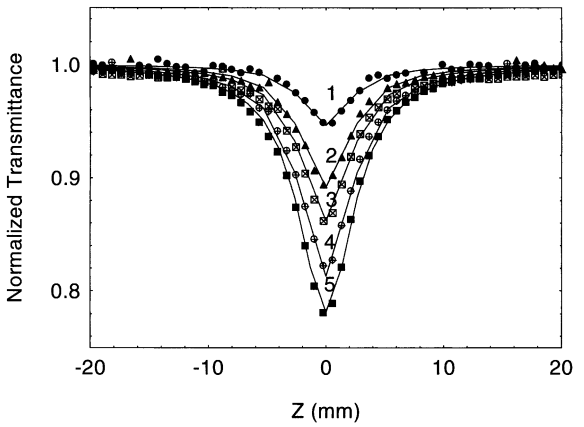

Fig. 3. *Z*-scan data for SD #2243 in ethanol. The linear transmittance is 0.8 and the thickness is 1 mm. The energies are: (1) 0.01 μJ, (2) 0.025 μJ, (3) 0.03 μJ, (4) 0.05 μJ and (5) 0.065 μJ. Solid lines are numerical fits using 3-level model ($S_0 \rightarrow S_1 \rightarrow S_{ex}$) and the following parameters: σ_{01} (532 nm) = 1.7×10^{-18} cm^2, σ_{ex} (532 nm) = 2.5×10^{-16} cm^2 and $\tau_2 = 2$ ps.

3.2. Pump–probe polarization measurements

Time-resolved pump–probe measurements allow us to resolve molecular relaxation processes in liquid and polymeric media. Results for SD #2243 and PD #2093 in ethanol and PUA are presented in Figs. 4–6. The main features of these pump–probe measurements are the following. Excitation of dye molecules with linearly polarized light leads to a polarization anisotropy of the first excited state (S_1) population for both ethanol solution and polymeric matrix samples. Decay kinetics as measured by probe polarizations parallel and perpendicular to the pump are not monoexponential since they include rotational motions as well as decay of the excited state S_1. The initial decay rate observed for parallel polarization is faster due to the combined effects of both mechanisms. The initial decay rate measured for perpendicular polarization is slower because molecules are rotating into the perpendicular orientation from parallel. At later times, after the anisotropy of the excited-state population has relaxed, all components show the same decay rate, i.e. that of the excited state. The probe decay is completely independent of polarization anisotropy when the probe is polarized at the "magic angle" (54.7°) with respect to the pump. The decay at this angle is monoexponential and corresponds to the lifetime τ_F of S_1. Experimental data for changes in transmittance for pump–probe polarizations oriented parallel, perpendicular and at the "magic angle" labeled $\Delta T_{\parallel}(t)$, $\Delta T_{\perp}(t)$ and $\Delta T_{magic}(t)$ are

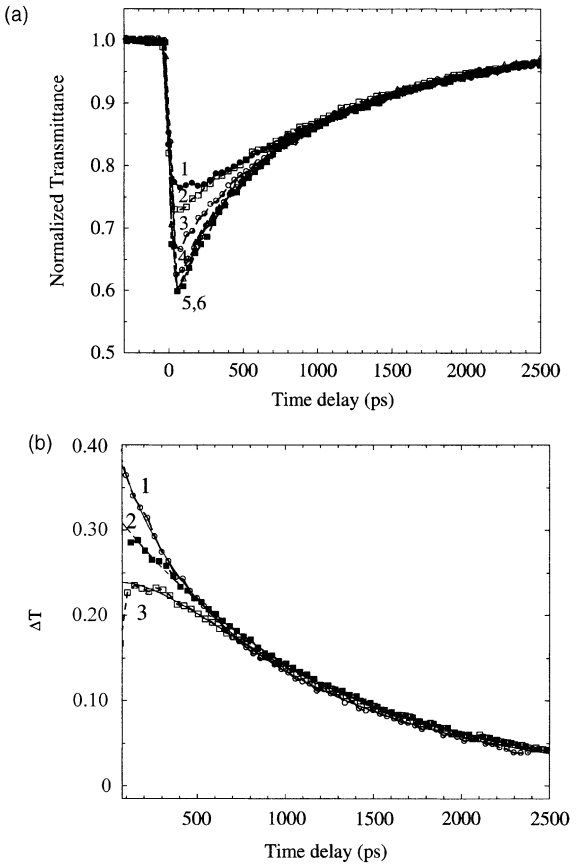

Fig. 4. Pump–probe measurements for SD #2243 in ethanol. Pumping energy is 0.8 μJ. The linear transmittance is 0.8 and the thickness is 1 mm. (a) The orientations of the probe beam relative to the pump are: (1) perpendicular, (2) 72°, (3) "magic angle" 54.7°, (4) 36°, (5) 18° and (6) parallel. Two last curves are almost overlapped. (b) ΔT results and their numerical fits (solid lines) for three orientations of the probe beam: (1) parallel, (2) "magic angle" and (3) perpendicular. Data for the "magic angle" were fitted using the single exponential decay expression: $\Delta T_{\text{magic}}(t) = \Delta T_{\text{magic}}(0)\exp(-t/\tau_{\text{F}})$. Parameters for this fit are: $\Delta T_{\text{magic}}(0) = 0.33$ and $\tau_{\text{F}} = 1200$ ps. Data for the parallel component were fitted using the double-exponential decay expression: $\Delta T_{\parallel}(t) = 0.33\exp(-t/1200)[1 + 2R(0)\exp(-t/\tau_{\text{R}})]$. Parameters for this fit are: $R(0) = 0.28$ and $\tau_{\text{R}} = 350$ ps. Data for the perpendicular component were fitted using the following double-exponential decay expression: $\Delta T_{\perp}(t) = 0.33\exp(-t/1200)[1 - 0.28\exp(-t/350)]$.

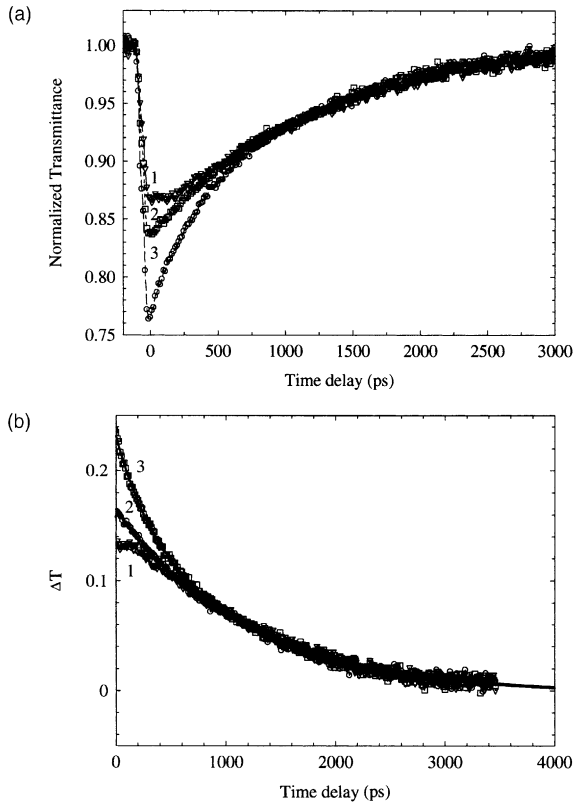

Fig. 5. Pump–probe polarization dependences for PD #2093 in ethanol. The linear transmittance is 0.9 and the thickness is 1 mm. Pumping energy is 1 μJ. (a) The orientations of the probe beam relative to the pump are: (1) perpendicular, (2) "magic angle" 54.7° and (3) parallel. (b) ΔT results and their numerical fits (solid lines) for three orientations of the probe beam: (1) parallel, (2) "magic angle" and (3) perpendicular. Data for the "magic angle" were fitted using the single exponential decay expression: $\Delta T_{\text{magic}}(t) = \Delta T_{\text{magic}}(0)\exp(-t/\tau_{\text{F}})$. Parameters for this fit are: $\Delta T_{\text{magic}}(0) = 0.17$ and $\tau_{\text{F}} = 1200$ ps. Data for the parallel component were fitted using the double-exponential decay expression: $\Delta T_{\parallel}(t) = 0.17\exp(-t/1200)[1 + 2R(0)\exp(-t/\tau_{\text{R}})]$. Parameters for this fit are: $R(0) = 0.2$ and $\tau_{\text{R}} = 380$ ps. Data for the perpendicular component were fitted using the following double-exponential decay expression: $\Delta T_{\perp}(t) = 0.17\exp(-t/1200)[1 - 0.2\exp(-t/380)]$.

shown in Figs. 4b and 5b. It was already shown [5] that for relatively small changes, ΔT is proportional to the excited-state population density. If ΔT is very large, the linear relationship between ΔT and excited-state population is lost and the decay no longer appears exponential. However, even for the largest transmittance change (~40%) observed in our measurements, the error this introduces in lifetime measurement is less than 10%, which is within experimental error. Therefore, the data for ΔT at the "magic angle" can be fit for

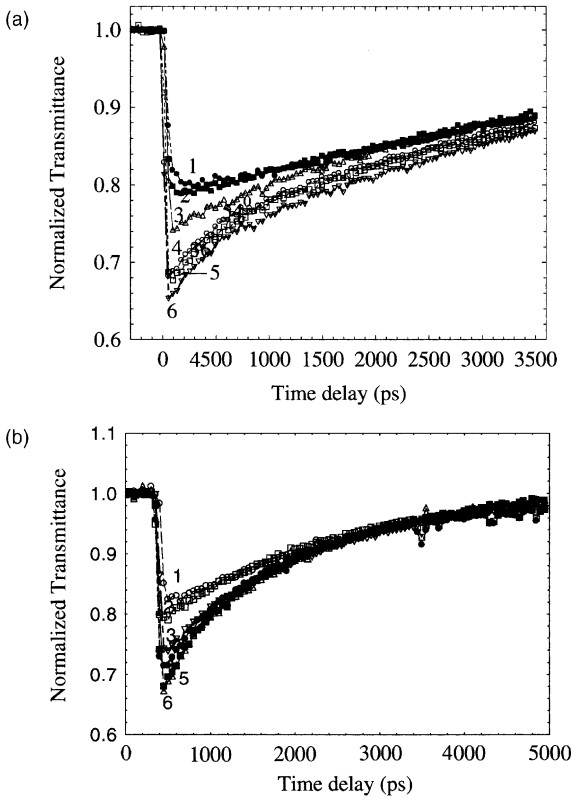

Fig. 6. (a) Pump–probe polarization measurements for SD #2243 in PUA. Pumping energy is 0.8 μJ. The linear transmittance is 0.8 and the thickness is 1 mm. The orientations of the probe beam relative to the pump are: (1) perpendicular, (2) 72°, (3) "magic angle" 54.7°, (4) 36°, (5) 18° and (6) parallel. Two last curves are almost overlapped. (b) Pump–probe polarization measurements for PD #2093 in PUA. Pumping energy is 0.75 μJ. The linear transmittance is 0.82 and the thickness is 1 mm. The orientations of the probe beam relative to the pump are: (1) perpendicular, (2) 72°, (3) "magic angle" 54.7°, (4) 36°, (5) 18° and (6) parallel. Two last curves are almost overlapped.

determination of τ_F using the following single exponential decay expression: $\Delta T_{magic} = \Delta T_{magic}(0) \times \exp(-t/\tau_F)$. From these fits, we obtain:

For SD #2243: $\tau_F(\text{ethanol}) = 1.2 \pm 0.2$ ns;
$\tau_F(\text{PUA}) = 3 \pm 0.5$ ns;

For PD #2093: $\tau_F(\text{ethanol}) = 1.2 \pm 0.2$ ns;
$\tau_F(\text{PUA}) = 2 \pm 0.4$ ns.

To estimate the reorientation times τ_R in ethanol we used the following double-exponential decays for $\Delta T_{\parallel}(t)$ and $\Delta T_{\perp}(t)$:

$$\Delta T_{\parallel}(t) = \Delta T_{magic}(0)\exp(-t/\tau_F) \times [1 + 2R(0)\exp(-t/\tau_R)], \quad (1)$$

$$\Delta T_{\perp}(t) = \Delta T_{magic}(0)\exp(-t/\tau_F) \times [1 - R(0)\exp(-t/\tau_R)], \quad (2)$$

where $R(0)$ is defined in the next section. As will be shown in the next paragraph, these expressions make it possible to achieve the complete separation of τ_R and τ_F. From fitting the decay curves shown in Figs. 4b and 5b, we found the following values of τ_R:

For SD #2243: $\tau_R(\text{ethanol}) = 350 \pm 50$ ps;

For PD #2093: $\tau_R(\text{ethanol}) = 380 \pm 50$ ps.

3.3. Anisotropy decay

In order to understand the nature of rotational motions in ethanol and PUA, it is useful to determine the decay of the anisotropy from the parallel and perpendicular nonlinear absorption data. The anisotropy $R(t)$ is defined in analogy to the definition for fluorescence anisotropy:

$$R(t) = [\Delta T_{\parallel}(t) - \Delta T_{\perp}(t)]/[\Delta T_{\parallel}(t) + 2\Delta T_{\perp}(t)]. \quad (3)$$

Inserting Eqs. (1) and (2) into Eq. (3) yields

$$R(t) = R(0)\exp(-t/\tau_R). \quad (4)$$

Thus, the transient pump–probe anisotropy method can be used to separate the population decay kinetics from the reorientational dynamics. In concentrated dye solutions the anisotropy decay kinetics may be effected by resonance energy transfer among molecules. This effect occurs if the distance, r, between molecules is close to a characteristic distance, the so-called Forster distance, R_0, which is typically equal to 4 nm for these types of molecules [8]. In our experiments the concentration of dyes both in ethanol and PUA does not exceed 10^{-3} M/l. Therefore, the distance between molecules (r) is at least 12 nm ($3R_0$). In this case the energy transfer efficiency, given by $E = R_0^6/$

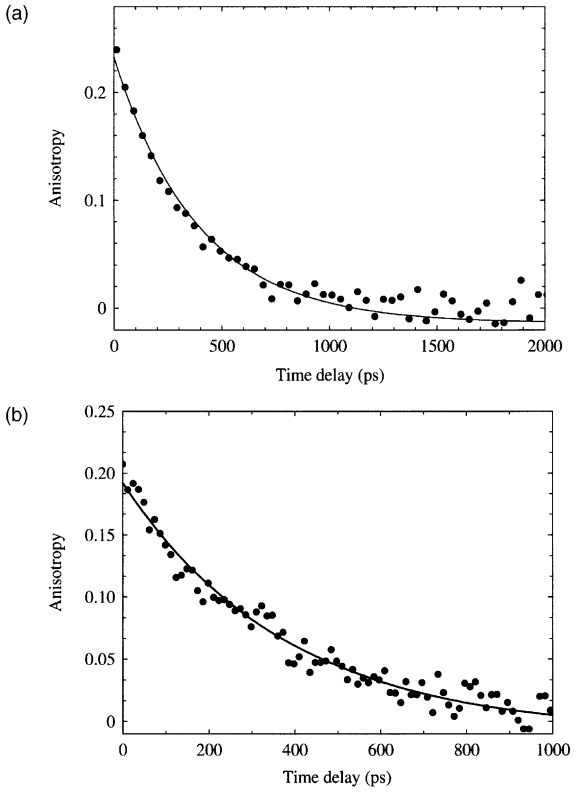

Fig. 7. (a) Anisotropy decay curve for SD #2243 in ethanol obtained from the data presented in Fig. 4a. The solid line is the numerical fit using the single-exponential decay expression: $R(t) = R(0)\exp(-t/\tau_R)$ with the parameters $R(0) = 0.28$ and $\tau_R = 350$ ps. (b) Anisotropy decay curve for PD #2243 in ethanol obtained from the data presented in Fig. 5b. The solid line is the numerical fit using the single-exponential decay expression: $R(t) = R(0)\exp(-t/\tau_R)$ with the parameters $R(0) = 0.2$ and $\tau_R = 380$ ps.

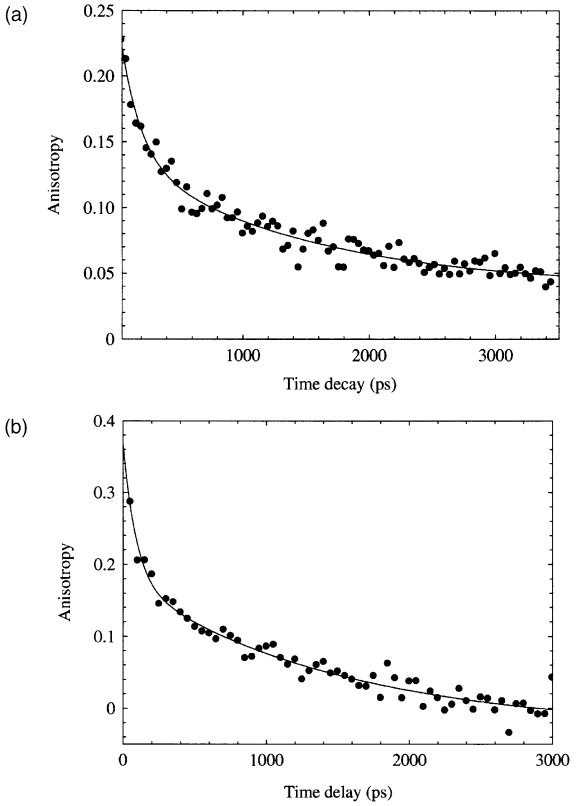

Fig. 8. (a) Anisotropy decay curve for SD #2243 in PUA obtained from the data presented in Fig. 6a. The solid line is the numerical fit using the double-exponential decay expression: $R(t) = a_1\exp(-t/\tau_{Rf}) + a_2\exp(-t/\tau_{Rs})$, where τ_{Rf} is the decay time of the fast component with amplitude a_1 and τ_{Rs} is the decay time of the slower component with amplitude a_2. Parameters for this fit are: $a_1 = 0.12$, $\tau_{Rf} = 150$ ps, $a_2 = 0.1$ and $\tau_{Rs} = 1400$ ps. (b) Anisotropy decay curve for PD #2093 in PUA obtained from the data presented in Fig. 6b. The solid line is the numerical fit using the double-exponential decay expression: $R(t) = a_1\exp(-t/\tau_{Rf}) + a_2\exp(-t/\tau_{Rs})$, where τ_{Rf} is the decay time of the fast component with amplitude a_1 and τ_{Rs} is the decay time of the slower component with amplitude a_2. Parameters for this fit are: $a_1 = 0.2$, $\tau_{Rf} = 100$ ps, $a_2 = 0.2$ and $\tau_{Rs} = 1500$ ps.

$(R_0^6 + r^6)$ [8], is less than 0.14%, which is a negligible value.

Anisotropy decay data together with fitting curves for SD #2243 and PD #2093 in ethanol and PUA are presented in Figs. 7 and 8. As can be seen, the anisotropy decay for both dyes in ethanol is monoexponential with decay time τ_R. Monoexponential anisotropy decay in ethanol for these dyes is evidence for allowed molecular motions leading to complete depolarization of the excited state. Anisotropy decay in PUA is described by two quite different exponential decay times. The coexistence of two very different decay times may be explained by the restriction of the fast decay process in the polymeric matrix permitting only a partial depolarization of the excited state. The loss of anisotropy in PUA is completed as a result of the slow relaxation process. The error bars for τ_R were estimated from the standard deviations of the average of several measurements. Under the approximation that the two anisotropy decay

times, τ_{Rf} (fast) and τ_{Rs} (slow), are very different (which we find to be the case for our situation) we can approximate the overall anisotropy decay by the sum of two exponential decays:

$$R(t) = a_1 \exp(-t/\tau_{Rf}) + a_2 \exp(-t/\tau_{Rs}).$$

The decay parameters for SD #2243 are: $\tau_R = (350 \pm 50)$ ps in ethanol; $\tau_{Rf} = (150 \pm 50)$ ps and $\tau_{Rs} = (1400 \pm 300)$ ps in PUA. For PD #2093: $\tau_R = (380 \pm 50)$ ps in ethanol; $\tau_{Rf} = (100 \pm 20)$ ps and $\tau_{Rs} = (1500 \pm 300)$ ps in PUA.

4. Discussion

Calculations of the optimized molecular geometry of PD #2093 show that this molecule is practically planar and exists in the ground state as an all-*trans* conformer, which is typical for PDs. Phenyl substitutes at the nitrogen atoms are situated almost perpendicular (>80°) with respect to the plane of the molecular moiety while the phenyl group at the meso-position of the polymethine chain is situated at an angle of nearly 60° to this plane. For the planar PD #2093 molecule the dipole moment is oriented straight along the direction of the polymethine chromophore and has a small value in the ground state.

SD #2243 exists in the ground state as a *cis* conformer of quasi-C_i symmetry, which is in accordance with Ref. [17]. CC-bonds in the central square group are lengthened (1.47–1.48 Å) in contrast to the typical conjugated CC-bond in the polymethine chromophore (1.40 Å). This leads to a deviation from the planar structure. Therefore, two parts of the chromophore form a dihedral angle of about 20° with respect to the axis defined by the two C=O bonds. As a result, the SD #2243 molecule has a dipole moment (larger than for PDs in the ground state) oriented perpendicular to this axis and not coincident with the direction of the chromophore. Calculated angles and bond lengths for SD #2243 are close to values published in Ref. [18].

Let us consider the possible rotational motions for SD #2243 and PD #2093 in ethanol solution. It is well known [8] that the rotational rate in solutions τ_R corresponds to the rotational correlation time θ, which is given by

$$\theta = \eta V/kT, \tag{5}$$

where η is the viscosity, V is the molecular volume of the rotating units, k is the Boltzmann constant and T is the temperature. An essential point is the knowledge of V. For estimation of this, we used 3D-quantum-chemical calculations described above. From our measurements of τ_R, Eq. (5) gives 1300 and 1400 Å^3 for SD #2243 and PD #2093, respectively. Comparison of these values with values obtained from quantum-chemical calculations may be used to study the nature of rotational motions.

In ethanol solution the SD molecule can form a solvent–solute complex due to intermolecular hydrogen bonds between the hydroxyl groups of the ethanol molecules and the central C_4O_2 unit [19]. Calculations show that the energy of formation of one hydrogen bond is 4 and 5.3 kcal/M for two hydrogen bonds with both oxygen atoms in the central group. These values are larger than kT at room temperature, which is the condition of the formation of stable complexes. It was previously shown that for related ketocyanines each oxygen atom could form two hydrogen bonds [20]. Therefore, we assume that the squarylium molecule forms a solvent–solute complex, which includes four molecules of ethanol connected to the dye molecule with hydrogen bonds. The energy of formation of four hydrogen bonds is 8.8 kcal/M. Calculations predicted practically the same solvent–solute formation energy in the excited state. This is because of the small changes in electron charges on the oxygen atoms ($0.01e$) during the excitation, while there are relatively large changes on the carbon atoms in the chromophore ($0.1e$). This would permit a solvent–solute complex to be stable in the excited state.

The solvent shell around the PD molecule is formed in the ground state due to the induced orientation of the solvent dipole moments around positive and negative charges distributed in the polymethine chain. In the excited state the charges on the atoms become opposite in sign which leads to reorientation of the solvent dipoles [21].

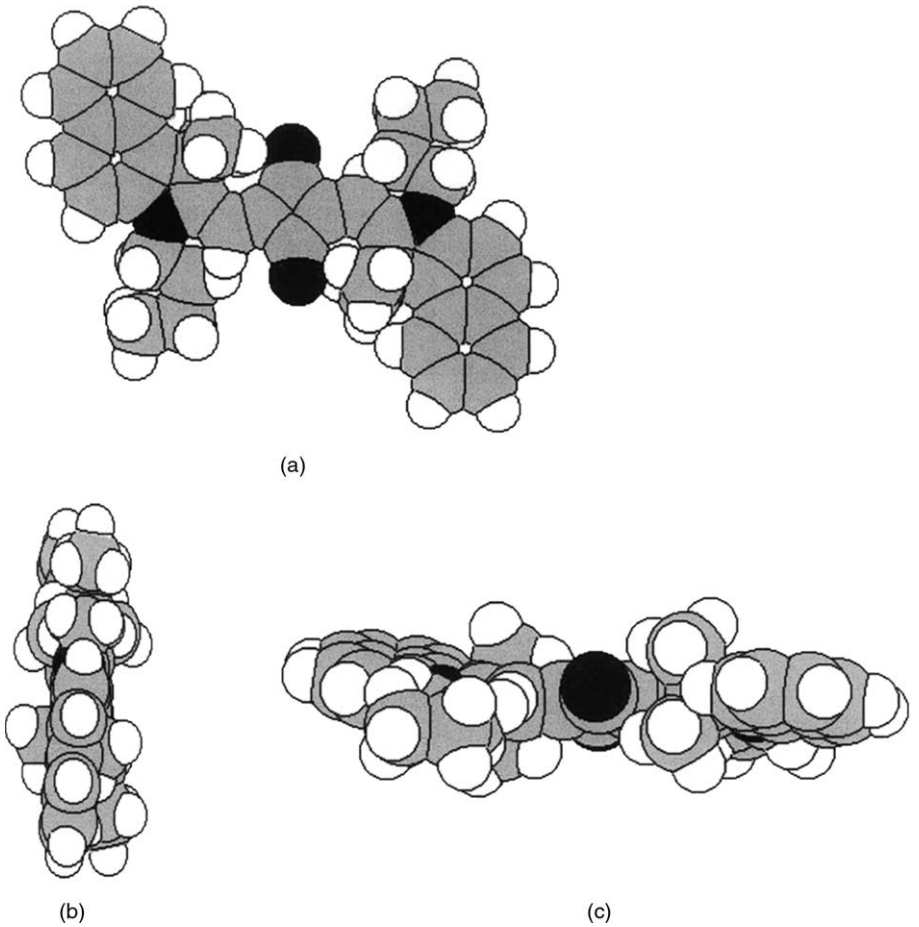

Fig. 9. Van der Waals model pictures for SD #2243 molecule in the plane (a) *XY*, (b) *YZ* and (c) *XZ*. Hydrogen atoms have white color, carbon atoms—gray, nitrogen atoms—black triangles and oxygen—black half spheres.

Molecular volumes for SD #2243 and PD #2093 were calculated as polyhedron volumes in the van der Waals model using the HyperChem software package. The thickness of the planar π-conjugated system is 3.4 Å. The volume contribution of every hydrogen atom was estimated as a half of a van der Waals ball with a radius of 1.09 Å; while a phenyl group in indolenine or benzoindolenine residues was estimated as a van der Waals ball of radius of 1.8 Å. The volume of the butyl (C_4H_9) substitute is equivalent to ≈3 methyl groups. An ethanol molecule could be considered as 3 connected balls with a total volume of ≈60 $Å^3$. In these approximations the van der Waals volume for SD #2243 is 450 $Å^3$ and for PD #2093 is 470 $Å^3$, i.e. they are nearly the same. Because SD #2243 exists as a solvent–solute complex with four ethanol molecules, its molecular volume is about 700 $Å^3$. Figs. 9 and 10 shows 3D images for these dye molecules.

It is therefore necessary to improve the correspondence between the τ_R calculated from Eq. (5) and the HyperChem package. We need to consider effective molecular volumes ≈1300–1400 $Å^3$ that are much larger than the corresponding van der Waals volume for PD #2093 and even larger than the volume of the solvent–solute complex for SD #2243. This difference may be attributed to interactions between dye molecules and the polar solvent. From our results we can conclude that the

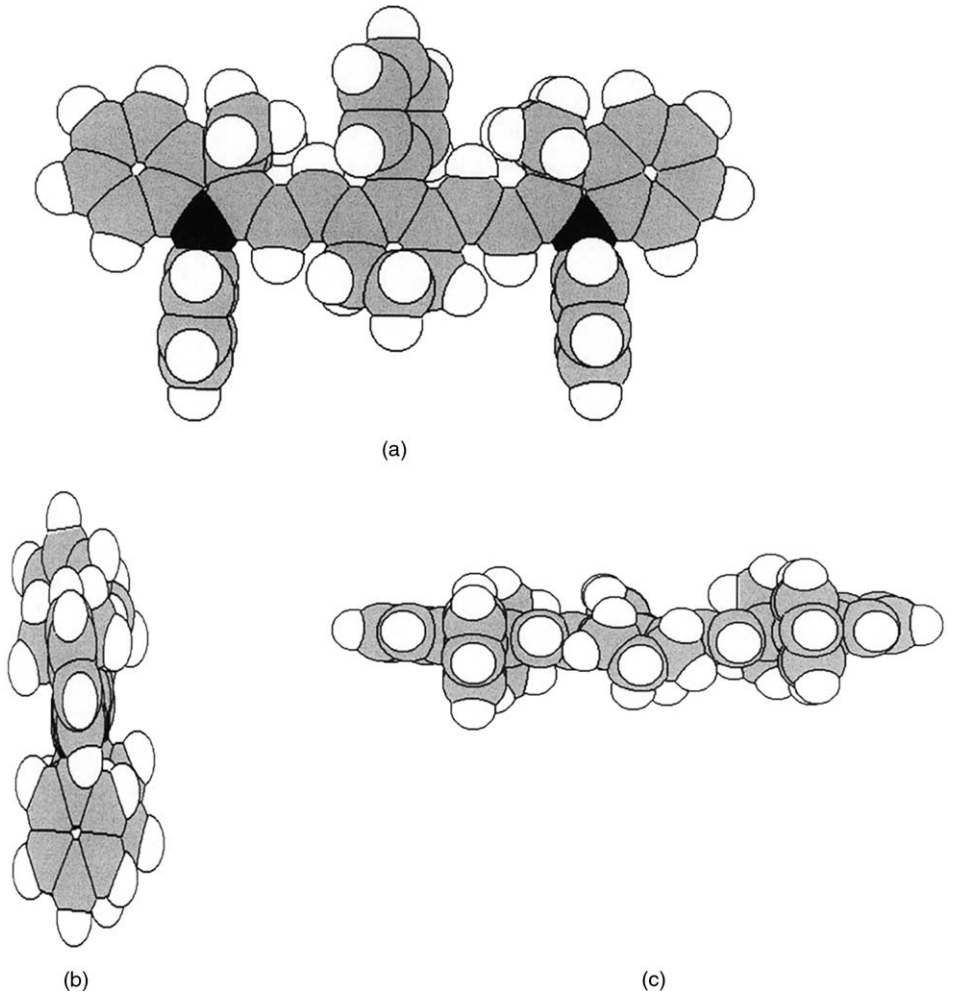

Fig. 10. Van der Waals model pictures for PD #2093 molecule in the plane (a) *XY*, (b) *YZ* and (c) *XZ*. Hydrogen atoms have white color, carbon atoms—gray and nitrogen atoms—black.

effective molecular volume of a rotating unit includes the dye molecule with about 15 solvent (ethanol) molecules forming the surrounding solvent shell. For SD #2243 some of the ethanol molecules can form intermolecular hydrogen bonds between the hydroxyl groups of the ethanol molecule and the central C_4O_2 group. Other ethanol molecules form a solvent shell. This case corresponds more to a ''stick'' boundary condition (where the first solvent layer rotates with the dye molecule) than to a ''slip'' condition (where the rotation is as in a vacuum) [8].

Our understanding of the nature of rotational motions in ethanol is the following. For PD #2093 the transition moment $S_0 \rightarrow S_1$ is directed along the symmetry axis (along the polymethine chromophore). Therefore, only rotation relative to the axis perpendicular to the plane of the molecule can change the direction of the dipole moment and lead to complete depolarization. For SD #2243 the transition moment $S_0 \rightarrow S_1$ forms an angle about 26° with respect to the molecular symmetry axis. In this case both rotations relative to the axis perpendicular to the plane of the molecule and to

the axis passing through the oxygen atoms can contribute to the loss of anisotropy.

Rotational motions in the PUA elastopolymer may be explained in a rather different way. During the polymerization procedure all dye molecules form local free volume cavities around themselves. Due to our method of photopolymerization and the elasticity of the medium, these microcavities may be especially easily formed. In the first approximation these cavities may be represented as cylinders, see Figs. 11 and 12. For SD #2243 the length of the cylinder corresponds to the distance between the hydrogen atoms farthest removed from the axis of rotation. We suppose also that nonrigid butyl substitutes at the nitrogen sites are packed into a cavity specified by the rigid part of the dye molecule. For PD #2093 the length of the cylinder corresponds to the distance between the farthest hydrogen atoms in the terminal groups, and the diameter of the cylinder is specified by the farthest hydrogen atoms of the phenyl groups placed near the nitrogen atoms and in a meso-position of the polymethine chain. This concept of cylindrical microcavities gives an idea of how a double-component depolarization decay of dyes within the polymer matrix may occur. It is logical to propose that the fast component may be connected with the rotation of molecular fragments. Calculations show that a rotation of 45° does not exceed the cylindrical volume. Due to these rotations the direction of the transition dipole moment changes by ~29° for SD #2243 and by ~28° for PD #2093. These rotations alone are insufficient for complete depolarization as was observed experimentally. Our measurements show that the fast rotational components for the polymer occur

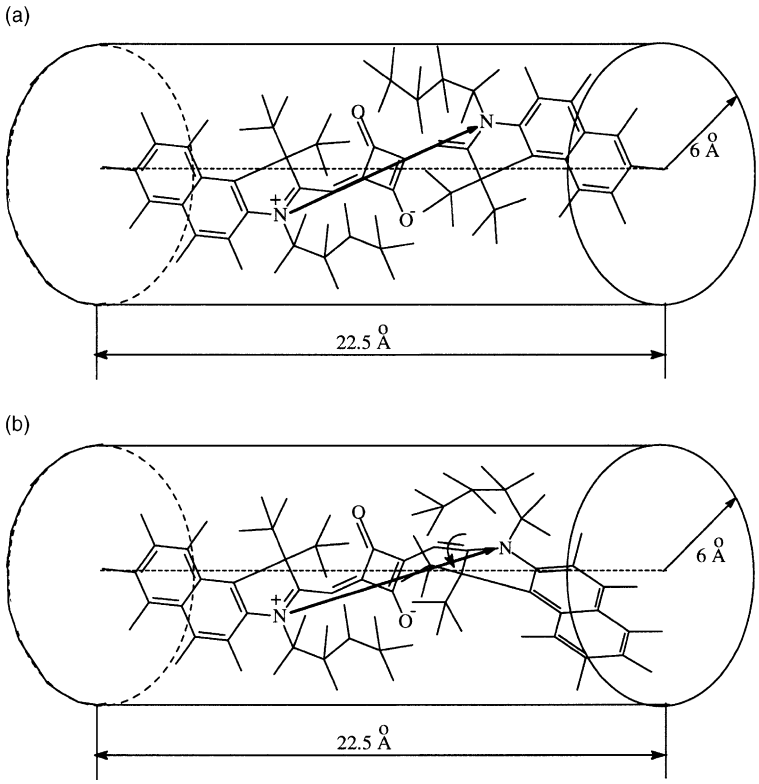

Fig. 11. (a) Polymer microcavities containing SD #2243 molecule and (b) its possible molecular motions. Solid black line between nitrogen atoms shows the orientation of the dipole moment. Dashed horizontal line is geometrical X-axis of the molecule. The arrow shows the precession of the dipole moment leading to partial depolarization.

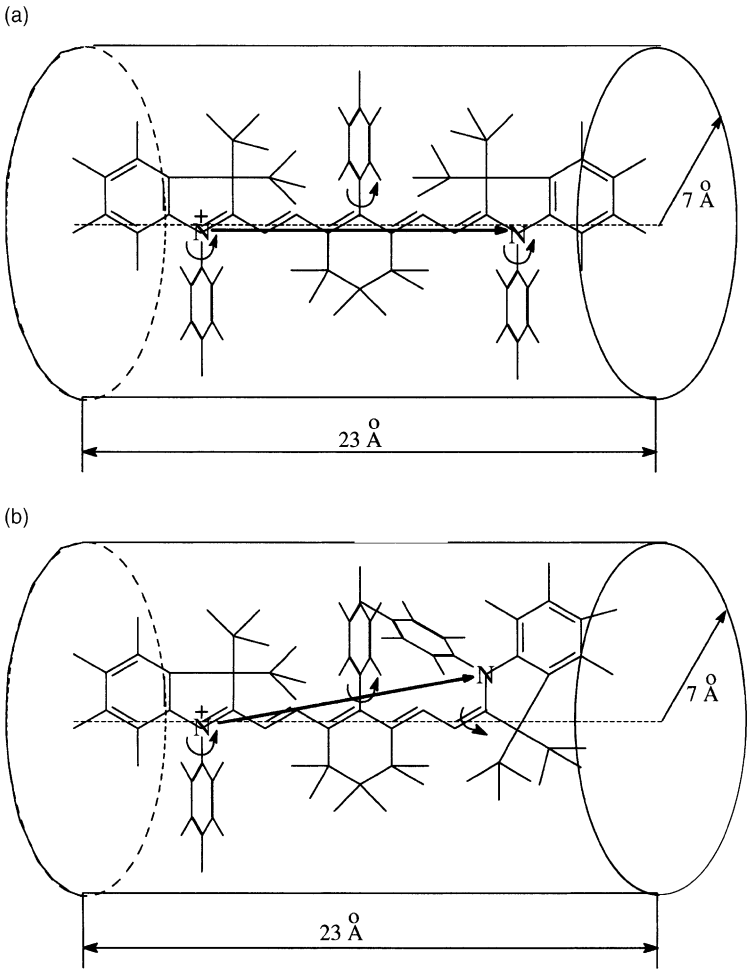

Fig. 12. (a) Polymer microcavities containing PD #2093 molecule and (b) its possible molecular motions. Solid black line between nitrogen atoms shows the orientation of the dipole moment. Dashed horizontal line is geometrical X-axis of the molecule. The arrows show the rotations of phenyl groups with the precession of the dipole moment leading to partial depolarization.

on a shorter time scale than in ethanol solutions. This fact supports the assumption that the rotational motions in the polymer are not restricted by solvent–solute interactions as in ethanol but are limited by the free volume of the microcavities. These possible rotations in polymer microcavities are shown schematically in Figs. 11b and 12b.

The second, slower component is probably connected with the rotation of the entire molecule in the microcavities due to the viscoelastic properties of the medium. It is known [15] that PUA exists at room temperature in a highly elastic state (the glass transition temperature is around -50 °C) which is associated with the faster segmental dynamics and microscale fluctuations of density compared to the glassy state. The PUA network of our material is characterized by a small degree of cross-linking (i.e. large distance between cross-links). It is logical to assume that nanosecond time scale fluctuations of the microcavity volume are responsible for a slower component in the decay kinetics leading to complete depolarization. These results are consistent with a study of reorientation of the molecules in different polymer

hosts performed by time-resolved fluorescence anisotropy measurements in Refs. [10,22]. They revealed a strong dependence of the residual anisotropy of the molecules on temperature and the degree of network cross-linking.

5. Conclusions

Picosecond measurements of the anisotropy of the nonlinear response in combination with quantum-chemical calculations and modeling give a variety of information about the molecular motions and rotational times in the different environments.

We have described detailed investigations of two organic dyes SD #2243 and PD #2093, which have attractive properties for optical limiting applications in ethanol solutions and the elastopolymer PUA. From anisotropy decay data we found the rotational times in ethanol: $\tau_R = (350 \pm 50)$ ps for SD #2243 and (380 ± 50) ps for PD #2093. These decays follow a single exponential decay that is evidence for the allowed molecular motions leading to complete depolarization of the excited state. The most likely mechanism of the reorientations is the rotation of dye molecules around the axis perpendicular to the plane of molecules that can substantially change the direction of the transition dipole moment. From the comparison of van der Waals volumes and volumes calculated from the experimental data, we assume that the rotation involves the nearest solvent shell. In contrast to the measurements in ethanol solution, anisotropy decays in PUA follow a double exponential behavior: $\tau_{Rf} = (150 \pm 50)$ ps and $\tau_{Rs} = (1400 \pm 300)$ ps for SD #2243, and $\tau_{Rf} = (100 \pm 20)$ ps and $\tau_{Rs} = (1500 \pm 300)$ ps for PD #2093. Possible rotations in the PUA matrix are connected with the existence of local microcavities of free volume formed around the dye molecules during the polymerization procedure. It is logical to assume that the fast subnanosecond components in PUA are connected with the rotation of molecular fragments in microcavities of free volume, and the slower nanosecond components are connected with the rotation of entire molecules due to fluctuations of free volume in the elastic medium. We expect that this methodology of combining nonlinear decay anisotropy measurements with quantum-chemical calculations and 3D modeling of dye structure may lead to progress in understanding the nature of rotational motions in the excited state and as a result to synthesis of new dyes with improved properties for nonlinear optical applications.

Acknowledgements

We gratefully acknowledge the support of the National Science Foundation (grant ECS# 9970078), the Office of Naval Research (grant number N00014-97-1-0936) and the Naval Air Warfare Center Joint Service Agile Program, contract number N00421-98-C-1327.

References

[1] O.V. Przhonska, J.H. Lim, D.J. Hagan, E.W. Van Stryland, M.V. Bondar, Y.L. Slominsky, J. Opt. Soc. Am. B 15 (1998) 802–809.
[2] J.H. Lim, O.V. Przhonska, S. Khodja, S. Yang, T.S. Ross, D.J. Hagan, E.W. Van Stryland, M.V. Bondar, Y.L. Slominsky, Chem. Phys. 245 (1999) 79–97.
[3] J.W. Perry, Organic and metal-containing reverse saturable absorbers for optical limiters, in: H.S. Nalwa, S. Miyata (Eds.), Nonlinear Optics of Organic Molecules and Polymers, CRC Press, New York, 1997, pp. 813–840.
[4] E.W. Van Stryland, D.J. Hagan, T. Xia, A.A. Said, Applications of nonlinear optics to passive optical limiting, in: H.S. Nalva, S. Miyata (Eds.), Nonlinear Optics of Organic Molecules and Polymers, CRC Press, New York, 1997, pp. 841–860.
[5] H.E. Lessing, A. Von Jena, Chem. Phys. Lett. 42 (1976) 213–217.
[6] A. Von Jena, H.E. Lessing, Chem. Phys. 40 (1979) 245–256.
[7] H.E. Lessing, A. Von Jena, Chem. Phys. 41 (1979) 395–406.
[8] J.R. Lakowicz, in: Principles of Fluorescence Spectroscopy, second edition, Kluwer Academic/Plenum Publishers, New York, 1999, p. 698.
[9] M. Levitus, J.L. Bourdelande, G. Marques, P.F. Aramendia, J. Photochem. Photobiol. A: Chem. 126 (1999) 77–82.
[10] A.P. Dorado, I.F. Pierola, J. Lumin. 72–74 (1997) 484–486.
[11] O.V. Przhonska, M.V. Bondar, J. Gallay, M. Vincent, Y.L. Slominsky, A.D. Kachkovki, A.P. Demchenko, J. Photochem. Photobiol. B: Biol. 52 (1999) 19–29.

[12] P.V. Poliakov, B.R. Arnold, Spectrosc. Lett. 32 (1999) 747–762.
[13] M. Assel, R. Laenen, A. Laubereau, J. Phys. Chem. A 102 (1998) 2256–2262.
[14] K. Das, A.V. Smirnov, M.D. Snyder, J.W. Petrich, J. Phys. Chem. B 102 (1998) 6098–6106.
[15] V.I. Bezrodnyi, M.V. Bondar, G.I. Kozak, O.V. Przhonska, Y.A. Tikhonov, J. Appl. Spectrosc. 50 (1989) 441–454.
[16] R. Negres, O.V. Przhonska, D.J. Hagan, E.W. Van Stryland, M.V. Bondar, Y.L. Slominsky, A.D. Kachkovski, IEEE J. Selected Topics Quantum Electronics, in press.
[17] L. Tong, P. Bi-Xian, Dyes Pigments 43 (1999) 73–76.
[18] R.W. Bigelow, H.-J. Freund, Chem. Phys. 107 (1986) 159–174.
[19] G.W. Scott, K. Tran, J. Phys. Chem. 98 (1994) 11563–11569.
[20] V.V. Danilov, G.G. Dyadusha, A.A. Rukov, Dokladu Akademii nayk SSSR (in Russian) 245 (1979) 639–643.
[21] A.D. Kachkovski, Russian Chem. Rev. 66 (1997) 647–664.
[22] A.D. Stein, D.A. Hoffman, C.W. Frank, M.D. Fayer, J. Chem. Phys. 96 (1992) 3269–3278.